A low-noise transimpedance amplifier for the detection of 'Violin-Mode' resonances in advanced LIGO suspensions

N.A. Lockerbie and K.V. Tokmakov

SUPA (Scottish Universities Physics Alliance) Department of Physics, University of Strathclyde, 107 Rottenrow, Glasgow G4 0NG, UK.

Abstract. This paper describes the design and performance of an extremely low-noise differential transimpedance amplifier, which takes its two inputs from separate photodiodes. The amplifier was planned to serve as the front-end electronics for a highly sensitive shadow-displacement sensing system, aimed at detecting very low-level 'Violin-Mode' oscillations in 400 μm diameter by 600 mm long fused-silica suspension fibres. Four such highly-tensioned fibres support the 40 kg test-masses/mirrors of the Advanced LIGO (Laser Interferometer Gravitational wave Observatory) interferometers. This novel design of amplifier incorporates features which prevent 'noise-gain peaking' arising from large area photodiode (and cable) capacitances, and which also usefully separate the *DC* and *AC* photocurrents coming from the photodiodes. In consequence, the differential amplifier was able to generate straightforwardly two *DC* outputs, one per photodiode, as well as a single high-gain output for monitoring Violin-Mode oscillations—this output being derived from the difference of the photodiodes' two, naturally anti-phase, *AC* photocurrents. Following a displacement calibration, the amplifier's final Violin-Mode signal output was found to have an *AC* displacement responsivity at 500 Hz of $(9.43 \pm 1.20)\ \mathrm{MV_{rms}.m_{rms}^{-1}}$, and, therefore, a shot-noise limited sensitivity to such *AC* shadow- (i.e., fibre-) displacements of (69 ± 13) picometres /√Hz at this frequency, over a measuring span of ±0.1 mm.

PACS numbers: 04.80.Nn, 84.30.-r, 06.30.Bp, 07.07.Df, 07.57.-c

1. Introduction

A prototype system of four shadow-sensors was designed to be retro-fitted into an Advanced LIGO (Laser Interferometer Gravitational wave Observatory) test-mass/mirror suspension, in which a 40 kg test-mass was suspended by four fused silica fibres, the dimensions of each fibre being approximately 600 mm long by 400 μm in diameter [1–6]. These shadow-sensors—one per suspension fibre—each comprised an optical emitter and detector, which bracketed the illuminated fibre. The emitter provided a collimated beam of illumination from a Near InfraRed (NIR: λ = 890 nm) multi-LED source, and this cast a vertical shadow of the illuminated fibre onto its facing, photodiode-based, detector. The detector was configured to monitor, with extremely high precision, any lateral displacement of the fibre's shadow. Ultimately, each detector was in the form of a differential 'synthesized split-photodiode'—this having a negligible dead-band between its pair of sensing photodiode elements [7,8,9]. The purpose of the full shadow-sensing detection system was first and foremost to monitor any lateral 'Violin-Mode' (*VM*) resonances that might be excited on these highly tensioned silica fibres at frequencies in the range 500 Hz–5 kHz, which spanned the gravitational wave detection bandwidth; and, as a secondary task, to record any 'large' amplitude 'pendulum-mode' motion of the test-mass and its suspension fibres at frequencies of ~ 0.6 Hz—such that all of this unwanted oscillatory motion, which might mimic or obscure the detection of gravitational waves, then could be suppressed by active cold-damping [10,11]. In consequence, the shadow-sensors were required to have a fibre- (i.e., a shadow-) displacement sensitivity of 10^{-10} m (rms)/√Hz at 500 Hz (the fundamental *VM* resonance frequency for the suspension fibres), over a ±0.1 mm range of lateral fibre position.

Initially, a transimpedance (photocurrent-to-voltage) amplifier was researched for use as the low-noise 'front-end' electronics to a single photodiode–based shadow-sensor, with the shadow of the illuminated fibre falling over one vertically-orientated edge of the rectangular sensor. In this way, a lateral displacement of the silica fibre's shadow altered the photocurrent flowing through the photodiode.

This single-photodiode-input amplifier, whose salient features are described in §2, subsequently was developed into a differential amplifier, which was interfaced to the split-photodiode based shadow-sensor, mentioned above. Here, the fibre's shadow fell over the central (common vertical) edge of two adjacent rectangular elements in the 'split-photodiode' detector. An additional, beneficial, side-effect of this combination of differential detector and amplifier was that proper shadow-alignment with the detector could be carried out more straightforwardly—by virtue of the natural pendulum-mode motion of the monitored fibre, in fact. This high-performance differential amplifier, now taking its inputs from a pair of photodiode elements, is described in §3. In both cases, the amplifier that would interface in a satisfactory way to its shadow displacement sensor was found to require some unusual features, as explained below in §2.

It turned out that vibrational motion of a silica fibre and its attendant shadow at a frequency of 500 Hz, and with an amplitude of 10^{-10} m (rms), equated to an *AC* photocurrent modulation at this frequency of approximately 4 picoamps (rms), flowing in anti-phase in each of the elements of a split-photodiode detector. However, it was conceivable that 'very large' Violin-Mode vibrations of up to 1 μm amplitude (2 μm peak-peak) might be excited in the suspension fibres, for which anti-phase currents of 40 nA amplitude necessarily would flow in a differential detector, and such signals clearly would have to be accommodated within the amplification chain as well—with neither distortion, nor clipping. In addition, pendulum-mode motion of a suspended test-mass, which certainly can undergo excursions of ±100 μm in the monitored fibre's position, would generate in a proportional way an anti-phase photocurrent modulation of amplitude 4 μA in each sensing element, this occurring at a very low frequency (~ 0.6 Hz); and finally, each photodiode element's standing *DC* photocurrent, arising from its steady illumination by the NIR source, was found to be ~ 50 μA. Therefore, ostensibly, the detection amplifier would have to be designed in such a way as to handle a very wide range of photocurrents. However, it was appreciated that this range could be reduced significantly, with other attendant benefits as described below, if the *DC* and 0.6 Hz photocurrents were handled separately.

2. The prototype single-input Violin-Mode amplifier

Initially, a dual output transimpedance amplifier was therefore researched, such that the *AC* modulated *VM* photocurrent and the standing *DC* photocurrent—plus any very low frequency modulation—would produce separate *AC* and '*DC*' output voltages, these outputs both being proportional to their respective photocurrents, although via different resistive transduction paths.

As regards the amplifier's primary *AC* output, it was a requirement of the detection system that it should be able to monitor a number of harmonics of the fundamental *VM* resonance frequency, since these Eigenmodes also could be excited on the silica fibres—perhaps up to the tenth harmonic.

Therefore, the shadow-sensor's prototype transimpedance amplifier needed the following characteristics: -

1. High gain over a *VM* (*AC*) bandwidth covering at least a frequency range of 500 Hz–5 kHz: a transimpedance gain of 120 MΩ would generate a 19.2 volt signal (peak-peak) at the maximum anticipated level of *VM AC* photocurrent. Such a signal would not necessarily saturate the amplifier, if it were powered from a conventional ±15 V power supply.
2. An ultra-low-noise level at the *VM* (*AC*) output over the frequency range specified in requirement 1, above. However, the photodiode(s) used necessarily had large detection areas, and concomitant capacitances, as well as long co-axial cable runs from these detectors (under ultra-high vacuum) to the amplifier itself—this being located some 6 m away outside the vacuum system. In total, the capacitance to *AC* ground at the amplifier's input would be ~ 1000 pF. Therefore, it was anticipated that 'noise gain peaking' would occur within the above bandwidth [12], whereby the amplifier's input noise voltage would be magnified by a factor ~ 100. Clearly, this effect would have to be mitigated in the amplifier's design, at the outset.
3. Very low *VM* (*AC*) signal gain at ~ 0.6 Hz, so that pendulum-mode motion of the test-mass/suspension would not interfere with *VM* detection at frequencies of 500 Hz, and above.
4. A separate *DC* output for (ultimately, each of) the photodiode element(s), with a composite shadow-displacement range capability of ±100 μm, say, which would be sensitive also to the anticipated ~ 0.6 Hz pendulum-mode motion of a test-mass/mirror and its suspension fibres. Here, a transimpedance gain of just 120 kΩ would give a quiescent output of magnitude 6 volts at the anticipated level of standing *DC* photocurrent; and then, a ~ 0.6 Hz pendulum-mode modulation with an amplitude of 4 μA would superimpose an easily discernible ±0.48 volt excursion about this quiescent value, for a pendulum-mode swing of ±100 μm.
5. In addition to the foregoing requirements, it was felt that any overload of the *VM* (*AC*) amplifier should occur with essentially symmetrical clipping at the amplifier's output, such that a (cold-) damping system still could apply (e.g., electrostatic) damping forces in these circumstances with the correct phase. In other words, the decelerating forces, which must be proportional to the instantaneous fibre velocities for cold-damping, still could be applied with the proper 90° phase-lead to the fibre positions in these high-Q systems ($Q \cong 6 \times 10^8$ [6])—the relative phase being based just upon the information supplied by the *VM* position sensor, even in overload, of course [11].

2.1. The single-photodiode transimpedance amplifier: design

A transimpedance amplifier with a single-photodiode input was designed to address the requirements listed 1–5 above, and its circuit diagram is shown in Figure 1(b), with a subsequent modification that was made to it shown in 1(a).

Circuits similar to that shown in Figure 1(b)—if taken from the photodiode detector up to the node bearing the label *V′*—have been described previously for the purposes of 'rejecting ambient light' [13], or for the 'control of ambient light' [14]. In this work, however, the op-amp based circuit shown in the Figure does not discard the *DC* photocurrent, but rather uses it in order to create a separate '*DC*' output channel—to be employed, ultimately

(i) for aligning the shadow onto a dual-photodiode sensor,

(ii) for calibrating the *DC*, and hence *AC*, sensitivities to fibre- (shadow-) displacement, and

(iii) for sensing the pendulum-mode motion mentioned above—also employed in (i).

In Figure 1 the full photocurrent I_{Photo} flowing through the photodiode detector has been decomposed explicitly into its steady and time-varying parts, such that $I_{Photo} = I_{DC} + i$. Here, I_{DC} represents the mean, quiescent, *DC* (plus any very low frequency pendulum-mode *AC*) photocurrent, whereas *i* represents any 'Violin-Mode' *AC* modulation of the photocurrent due to lateral vibration of the monitored silica fibre, and its attendant shadow. In Figure 1(b) the non-inverting 'debout' (i.e. non-inverting) integrator feedback involving IC2, and its two resistors R, and capacitors, C, forces the *mean*, steady-state, *DC*, output of IC3 always to be close to zero volts, even though relatively large amplitude HF (High Frequency: in this context meaning frequencies ≥ 500 Hz) *AC* signals *V*′ also may be present at this node. A zero-average input to the integrator can occur only when no *DC* (photocurrent) flows through the resistor, R_f, and under these conditions the output of IC2, labelled V_{DC} in the Figure, must be frozen at whatever happened to be its existing—negative—value at the time the 'zero volts average' condition was achieved, at the output of IC3. Accordingly, the full *DC* photocurrent, I_{DC}, must flow down through resistor R_i from the anode (A) of the photodiode,

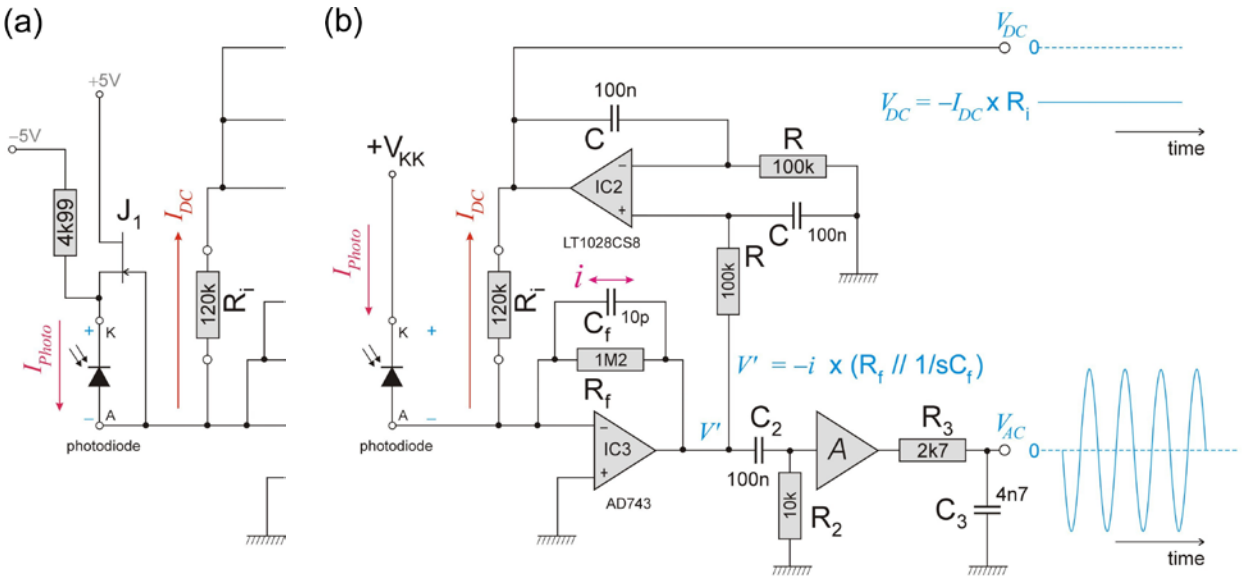

Figure 1. Schematic of the single-input amplifier. (a) Shows a subsequent modification made to the amplifier shown in (b). This involved 'bootstrapping' any signal present at the (large area) photodiode's Anode (A) to its Cathode (K), via the source-follower J_1. This prevented any signal current from flowing through the capacitance of the photodiode and its connecting cable: please refer to the text. Here, a small reverse bias V_{KK} ~ 0.5 V appeared across the photodiode. (b): 'Debout,' or non-inverting, integrator feedback via IC2 (together with the two resistors labelled R, and the two capacitors labelled C), forced the *mean* output voltage *V*′ of IC3 always to be close to zero volts, causing the *DC* and 'Violin-Mode' *AC* components of the photocurrent, I_{DC} and *i*, respectively, to follow the different paths indicated in the Figure (please refer to the text). The voltage gain *A* = 101.

which is a virtual Earth point (at the inverting input to IC3), into the output of IC2, which acts as a *DC* current-sink. Thus, $V_{DC} = -I_{DC} \times R_i$, as indicated in the Figure, and the *DC* transimpedance gain of the amplifier is therefore 120 kΩ.

In contrast, none of the *AC* photocurrent *i* can flow through resistor R_i, because the output of the sluggish integrator IC2 cannot follow this HF signal, so as to produce a suitable driving voltage for it across resistor R_i—due the long RC time-constant of integration. However, the output of transimpedance op-amp IC3 is free to respond to this HF photocurrent, by taking up an *AC* voltage at its output given by $V' = -i \times$ [impedance of $R_f // C_f$]. Indeed, for frequencies f below the pole frequency of the paralleled resistor-capacitor combination [$R_f // C_f$], i.e., for f < 13.2 kHz, any *AC* photocurrent *i* must flow essentially through the

transimpedance resistor R_f, alone. Thus, the *AC* transimpedance gain of this amplifier is 1.2 MΩ.

Therefore, overall, the non-inverting integrator feedback forces the *DC* and 'Violin-Mode' *AC* photocurrents to follow the different paths indicated in the Figure.

In the circuit of Figure 1(b) the *AC* signal *V'* is *AC* coupled—for frequencies above ~160 Hz—by the high-pass filter C_2–R_2 to the input of a voltage amplifier having a gain of A = 101 (for this single-photodiode amplifier), before being additionally band-limited in its frequency response on the high-frequency side by the low-pass filter R_3–C_3, which has a single-pole roll-off above 12.5 kHz.

In practice, it was the output of this filter which became the final 'Violin-Mode' output voltage of the amplifier, V_{AC}, as indicated in Figure 1. The mean value of the voltage *V'* being zero, together with the subsequent capacitive coupling to the voltage amplifier of gain A, ensured that large *AC* signals at the output of IC3 saturated symmetrically at this, and the following amplifier's, output. There was no large, negative, *DC* offset at IC3's output—causing asymmetrical saturation and clipping— due to a standing *DC* photocurrent flowing through resistor R_f. Moreover, this arrangement also permitted a larger value to be used for R_f, without saturating IC3's output at (essentially) the negative supply rail, thus ensuring a better (Nyquist) signal-to-noise ratio at the output of IC3: the *VM* signal $\propto R_f$, whereas the Nyquist noise $\propto \sqrt{R_f}$, so that the signal-to-noise ratio is maximised in this regard by making R_f as large as possible. Instead, photocurrents 'near *DC*' flowed through the conversion resistor R_i. In both the single-input and the subsequent dual-input differential amplifier of this work, the ratio $R_f/R_i = 10$, so that the overall *AC* transimpedance gain ≅ 1000× the *DC* transimpedance gain, mid-band.

2.2. The transimpedance amplifier: reducing input capacitance

The photodiode (PD) which was eventually chosen as the actual shadow-sensor was the *Hamamatsu* S2551 silicon device [15], having an effective detection area measuring 1.2 mm × 29.1 mm. Because of its large area (~ 35 mm^2), this PD had a relatively large capacitance: 350 pF, at zero bias. However, as a consequence of an additional capacitance of 600 pF, or more, in parallel with the PD, due to a necessary coaxial cable run of ~ 6 m between the photodiode(s) and the amplifier, a total input capacitance of C_{in} ~ 1000 pF was anticipated, as mentioned above. Therefore, the necessarily small value of feedback capacitance C_f (= 10 pF) meant that this was, unfortunately, an ideal configuration for 'noise gain peaking'—where the input voltage noise of op-amp IC3 is effectively multiplied-up by a factor of $1 + C_{in}/C_f$ (~ 100, here) [12].

This undesirable effect was mitigated firstly by choosing a low-noise op-amp for IC3 (initially an AD743: 5.0 nV/√Hz, max., at 1 kHz; and later, because of its much smaller SMD footprint, an OPA627AU: 5.6 nV/√Hz, typ., at 1 kHz); and secondly by adding the circuitry shown in Figure 1(a), which followed a scheme described in reference [12]. The prototype amplifier's original input circuit, shown in Figure 1(b), therefore was modified by the addition of the very low-noise JFET transistor, J_1 (BF862: ~ 1 nV/√Hz), connected as a source-follower, along with its simple biasing circuitry. This transistor 'bootstrapped' the signal from the photodiode's Anode (A)—such that any signal present at this 'virtual-earth' point (arising from IC3's falling open-loop gain with rising frequency) was transferred to the photodiode's Cathode (K), so that very little signal voltage now appeared *across* C_{in}. Consequently, a correspondingly reduced signal current now would be able to flow through the capacitance of the photodiode and its connecting cable—making them appear very much reduced in capacitance, and so greatly diminishing any noise gain peaking. The presence of

transistor J_1 also provided a small but useful reverse bias to the photodiode (~ 0.5 V), which slightly decreased its capacitance. The biasing arrangement shown in Figure 1(a) resulted in a standing current of approximately 1.1 mA flowing from J_1's source down through the 4k99 resistor to the regulated low-noise −5 V voltage rail.

The addition of the transistor J_1 did not alter either the *DC* or *AC* signal behaviour of the single-input amplifier, and so, from Figure 1(b), its '*DC*' output signal can be expressed straightforwardly in terms of the complex frequency s [$s = j\omega$, $j \equiv \sqrt{(-1)}$], by a transimpedance relationship of the form

$$\frac{V_{DC}}{I_{DC}} = -\frac{R_f}{\left(s^2 C R C_f R_f + sCR + R_f/R_i\right)}. \qquad (1).$$

Clearly, for a truly *DC* component of photocurrent ($s = 0$) Equation 1 reduces to the simple expression $V_{DC} = -I_{DC} R_i$, as mentioned above. For the component values given in Figure 1(b), the expression in Equation 1 is effectively that of a low-pass response, with a dominant pole at 161 Hz (and a second, HF, pole at 13.1 kHz): 0.6 Hz 'pendulum-mode' signals therefore were passed without attenuation, as '*DC*'.

In a similar fashion, the *ratio* of the amplifier's *AC* response to a *VM* signal photocurrent, to its *DC* response to a steady quiescent photocurrent (a convenient ratio) can be found to be

$$\frac{V_{AC}}{V_{DC}(s=0)} = \frac{A(R_f/R_i)s^2 C R C_2 R_2}{\left(s^2 C R C_f R_f + sCR + R_f/R_i\right)(sC_2R_2 + 1)(sC_3R_3 + 1)}. \qquad (2).$$

Here: $A = 101$, $C_f = 10$ pF, $R_f = 1.2$ MΩ, $R_i = 120$ kΩ, $C = 100$ nF, $R = 100$ kΩ, $C_2 = 100$ nF, $R_2 = 10$ kΩ, $C_3 = 4.7$ nF, and $R_3 = 2.7$ kΩ.

Equation 2 effectively expresses the relative sensitivity of the amplifier's *AC* and *DC* outputs to changes in photocurrent due to *the same* displacement of a fibre's shadow across (the edge of) a PD detector: in the *AC* case a change occurring at a frequency s (= $j\omega$) for a sinusoidal modulation at angular frequency ω; and in the *DC* case a change occurring from one steady *DC* value to another, as the fibre's shadow made a quasi-static displacement. Practically, this relationship was used to predict the sensitivity to *VM* displacement of the fibre, at any given frequency f (= $\omega/2\pi$), relative to the—straightforwardly measurable—rate of change of *DC* output voltage V_{DC} with silica fibre (shadow) position. Please refer to Figure 5.

In practice, the theoretical mid-band (~ 1.48 kHz) *AC*/*DC* gain ratio given by Equation 2 did not quite peak at the anticipated value of 101 × 10 = 1010, but was slightly reduced by the sharply circumscribed (four poles/two zeroes) pass-band of the amplifier.

2.3. Prototype amplifier: practical Near InfraRed (NIR) gain calibration

A calibration system was built to verify that Equation 2 properly described both the *AC* and *DC* behaviours of this amplifier. This system involved irradiating the amplifier's single photodiode detector with a very low intensity beam derived from an OD50L NIR LED, using a pin-hole aperture, the beam consisting of a steady component of fixed intensity, plus a small sinusoidal intensity modulation on top of this at a known frequency, f [16].

The results of such measurements of the *AC/DC* gain ratio as a function of the frequency f agreed with the theoretical expression given by Equation 2 at a ±1% level up to ~ 100 kHz, i.e., well above the required *VM* bandwidth of 5 kHz. Consequently, as mentioned above, a bench measurement of the shadow-sensor's quasi-static responsivity to shadow- (i.e.

suspension fibre-) displacement (hereinafter called the '*DC* slope sensitivity'), allowed the corresponding *AC* sensitivity to be inferred with a high degree of confidence from the measured *AC*/*DC* gain ratio at any given *VM* frequency, *f*. This was the technique used to calibrate the amplifier's '*AC* slope sensitivity,' as a function of *f* [17]. In practice the gain was found to be 1000 at 1.48 kHz, and 990 at 1 kHz (and 976 ±4 mid-band for the differential amplifier, described below, at 1.48 kHz).

3. The differential Violin-Mode amplifier

Following the successful performance of the prototype amplifier, connected to a single rectangular photodiode sensor, it was felt that a differential sensor would improve the signal-to-noise ratio. Two closely adjacent *Hamamatsu* S2551 photodiode elements, orientated so that the fibre's shadow fell along their common vertical edge, and sensing differentially, could in principle double the size of the available *AC* photocurrent signal, whilst offering a degree of common-mode rejection, as well. Clearly, a differential amplifier was needed, and in this case the overall signal-to-noise ratio was expected to improve over that of the single-input amplifier by a factor of $\sqrt{2}$, if the differential amplifier's noise performance turned out to be limited by fundamental, uncorrelated, shot noise arising from the *DC* photocurrents flowing in its two sensor elements.

3.1. The differential amplifier: from concept to construction

The outline design of the Transimpedance Amplifiers block (in what follows called simply 'the differential amplifier,' as above) is shown in Figure 2. It is essentially a dual version of the prototype amplifier, with an intermediate differential *AC* amplification stage. A very minor change from the prototype amplifier was that this stage had a (differential) voltage gain of $A = 100$, rather than a single-input gain of $A = 101$. This small change nevertheless had a measurable influence. For the photodiode element PDa in Figure 2, I_a represents the '*DC*' value of its photocurrent, inclusive of any pendulum-mode modulation, whilst i_a represents any HF modulation of this photocurrent due to transverse *VM* oscillation of its monitored fibre (and shadow). Similar nomenclature has been used for element PDb. Note that the modulation photocurrents i_a and i_b flowed automatically in anti-phase for the

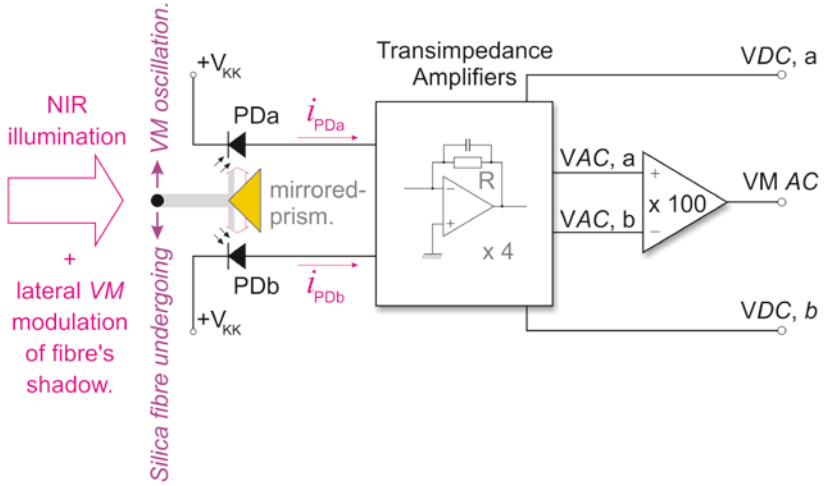

Figure 2. Schematic diagram of the Violin-Mode shadow-sensor connected to its 'Transimpedance Amplifiers' block (differential amplifier), with the 'synthesized split-photodiode-' based sensor being shown in plan view. The mirrored prism split the collimated incident NIR illumination so that it, together with a variable fraction of the fibre's shadow, fell onto each photodiode sensor element—as if the separate photodiodes formed a single split-photodiode detector, with negligible dead-band between the two elements. Here, the full photocurrents flowing in photodiode elements PDa and PDb have been designated, respectively, $i_{PDa} = I_a + i_a$ and $i_{PDb} = I_b + i_b$. Please refer to the text.

'synthesized split–photodiode' detector: if the silica fibre's shadow moved over the common edge of elements PDa and PDb, so as to move off PDa (by any amount) the illumination of PDa, and thereby its photocurrent, i_{PDa}, increased; but as the shadow moved off element PDa it moved automatically onto element PDb, thereby decreasing i_{PDb} by closely the same amount by which i_{PDa} was increased [17]. The amplifier's two '*DC*' voltage outputs, labelled *VDC,a* and *VDC,b* in the diagram, were derived from the *DC* photocurrents I_a and I_b, respectively, via a transimpedance gain of R = 120 kΩ. Similarly, the intermediate *AC* signal voltages *VAC,a* and *VAC,b* were derived from i_a and i_b, but in this case via a ten-times-larger transimpedance gain of R = 1.2 MΩ, as used in the single-input amplifier. These two transimpedance signals were then differenced, and their resulting differential voltage was amplified further by a factor of ×100, so as to produce the final Violin-Mode output voltage, VM *AC*. In this way, and measured from an individual photodiode element to its own respective pair of outputs, the overall, theoretical, *AC* transimpedance gain was found to be (976 ±4) × the *DC* gain (mid-band), or approximately 1 % lower than that of the single-input amplifier, as expected, given the slightly lower value of the *AC* gain stage in this amplifier.

The full circuit diagram of the differential amplifier is shown in Figure 3, and the realization of two such amplifiers on a pair of small Printed Circuit Boards, using surface-mount

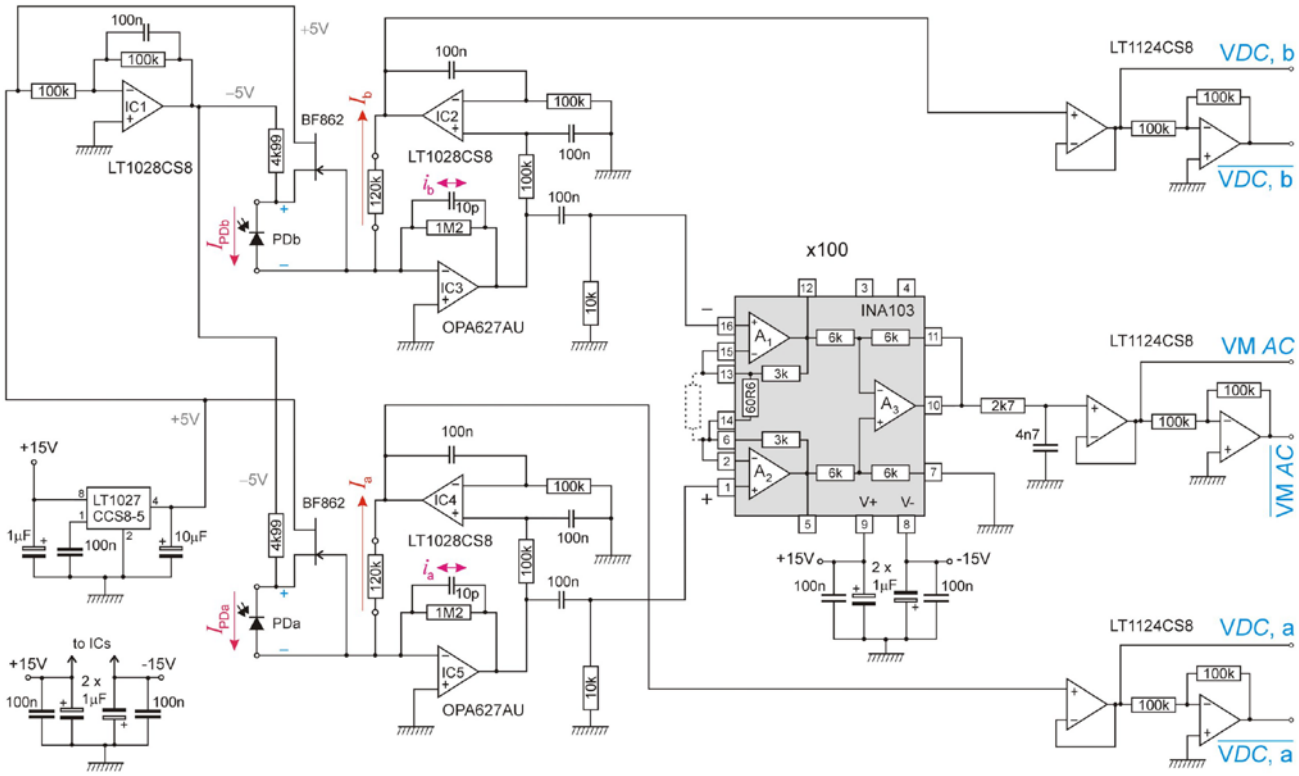

Figure 3. Circuit diagram of the Violin-Mode differential shadow-sensing transimpedance amplifier sensor (with photodiode sensing elements PDa and PDb). Three complementary outputs were made available for driving long cables, if necessary (please refer to the text). This also allowed positive versions of the two *DC* outputs, $\overline{VDC,a}$ and $\overline{VDC,b}$, to be used. The INA103 instrumentation amplifier is a 1 nV/√Hz device. Four such amplifiers were constructed—one per silica fibre. Two of these amplifiers are shown, as constructed, in Figure 4.

components, is shown in Figure 4. It is noteworthy that an earlier version of the differential amplifier, which was built using through-hole mounted components, gave an equally good noise

performance in the pass-band, but did not conform quite so closely to the theoretical high frequency performance as did the surface-mount amplifiers, as exemplified by Figure 5. Four differential, surface-mount, *VM* amplifiers and shadow-sensors were built, with one dual-photodiode based sensor plus one differential amplifier being dedicated to each suspension fibre of a full test-mass mirror suspension.

3.2. The differential amplifier: signal and noise performance

A typical noise Power Spectral Density (PSD) of the differential amplifier, measured at its VM *AC* output, is shown in Figure 5. The –3 dB bandwidth was found from a fit of Equation 2 to these noise data to lie between 226 Hz to 8.93 kHz. The theoretical pass-band is indicated by the labelled solid (blue) line in the Figure, and it is seen to be a very good fit to the measured noise PSD for frequencies above ~ 50 Hz. Moreover, the peak, mid-band, noise PSD was found to lie very close indeed to the fundamental shot-noise limit, as indicated in the Figure by the horizontal (red) line. Here, this limit was calculated from the two measured *DC* photocurrent values by assuming that the shot noise arising from the two photodiode elements was uncorrelated.

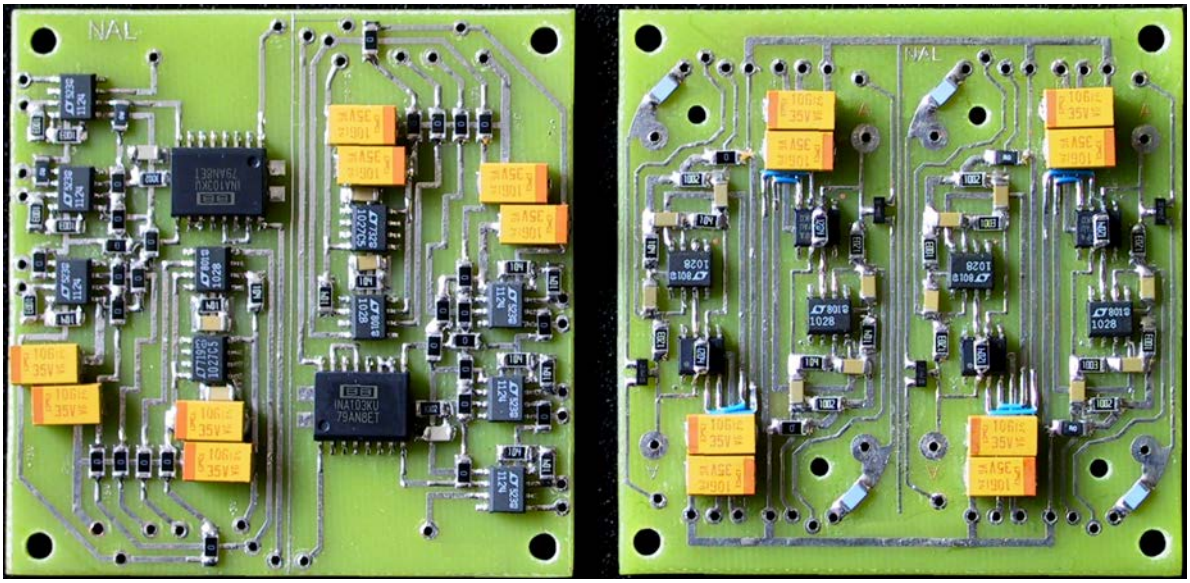

Figure 4. Two of the four SMD-based amplifiers were constructed on the pair of PCBs shown in the Figure, each amplifier being of the type shown in Figure 3. The PCBs measured 60 mm × 60 mm, such that they could be stacked one above the other within a compact square enclosure. Each amplifier was interfaced to a particular (differential photodiode based) shadow-sensor, a separate sensor being dedicated to each one of the four suspension fibres of a full test-mass/mirror suspension.

The roll-off of the amplifier's gain towards both lower and higher frequencies was at a rate of –40 dB/decade, and so the equivalent noise bandwidth was only slightly (a factor of $\pi/2\sqrt{2} = 1.11$) larger than the –3 dB bandwidth quoted above. Indeed, the steep roll-off towards *DC* meant that the signal gain (from Equation 2) was usefully very much smaller at the pendulum-mode frequency of 0.6 Hz than mid-band for *VM* signals—by a factor > 70,000, in fact. Given the measured mid-band noise PSD of –63.2 $dBV_{rms}/\sqrt{Hz}$ ($\equiv 692\ \mu V_{rms}/\sqrt{Hz}$), the broad-band rms noise voltage was expected to be $((8930 - 226) \times 1.11)^{1/2} \times 692\ \mu V = 68$ mV (rms). Indeed, this was very closely the rms level that was measured, as seen in Figure 6. As the rms value and standard deviation σ of Gaussian (shot) noise are equal, the anticipated visible 'band' of noise seen on the oscilloscope screen was expected to be ~ 4σ wide, or approximately 280 mV peak-peak—as indicated by the

horizontal bars in this Figure. Please note that the split supply rails for the amplifiers both benefited from 'noise finessing' filters, in order to reduce voltage regulator noise [18].

An actual *VM* signal resulting from an approximately 1 µm peak-peak acoustically-induced fibre resonance, at a frequency of 1019.1 Hz, is also shown in Figure 6. Here, the captured *VM AC* signal is seen to be approximately 10 volts, peak-peak.

In comparison, the maximum undistorted sinusoidal *VM* output signal was found to be 23 volts peak-peak (approx. 2.4 µm, peak-peak), although, were it ever to become necessary, this range could have been increased to > 27 V peak-peak, simply by running the entire circuit from ± 18 V (rather than ± 15 V) supply rails.

3.3. The differential amplifier: DC and AC slope sensitivities

In practice, quasi-*DC* pendulum-mode signals were detected using the *DC* outputs of these amplifiers, and signals with amplitudes of up to ±140 µm, peak-peak, at 0.64 Hz, were detected [9]. These same *DC* outputs were used also for displacement calibration, and in bench tests the *DC* responsivity, or 'slope sensitivity,' of each photodiode detector +

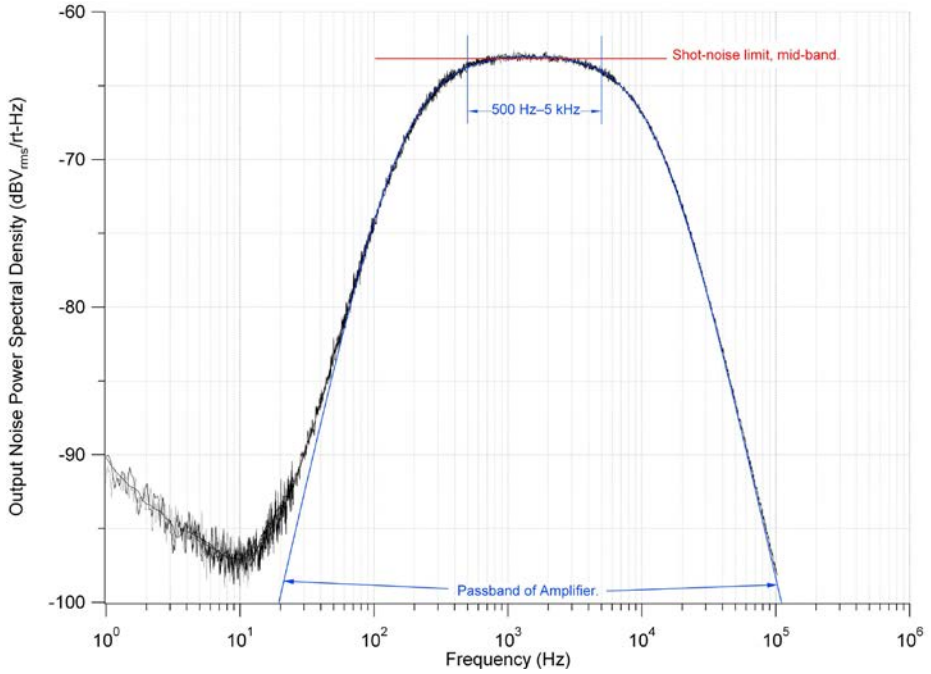

Figure 5. Noise Power Spectral Density of the differential amplifier as a function of frequency, measured at the *VM AC* output of the amplifier. The fundamental mid-band shot noise limit is marked by the horizontal line in the Figure, at –63.2 dBVrms/√Hz. The theoretical amplifier Passband, as described by Equation 2, is indicated by the blue line. Here, the fibre's shadow fell over neither detector element, in order to avoid *VM* and other resonant peaks, and so the noise PSD is higher in this Figure at 500 Hz, say, than when the shadow fell over the adjacent edge of both elements—as it must for proper *VM* detection. The reduction in noise PSD with the shadow present was approximately 0.8 dB, in fact. It was due entirely to the lower levels of *DC* photocurrent, and so shot noise, in the two partially shaded PD elements [7].

amplifier was measured by translating laterally a test fibre, mounted vertically on a motorised stage, through the NIR beam of each shadow sensor. The shadow of the fibre, falling firstly onto one and then onto the other adjacent photodiode element in each sensor, caused successive 'notches' to appear in their *DC* outputs. At the end-of-span 'cross-over' region (ξ = ±0.1 mm), where the shadow was still passing from one element onto the other, the rate of change of the differential *DC* voltage with fibre position ξ, i.e., the *DC* slope

sensitivity [$\equiv \partial(VDC, a - VDC, b)/\partial\xi$], was found [17]. Taken over the four detectors and their respective amplifiers, it was measured to be 10.44 $kV.m^{-1}$ of fibre displacement. From this value, the corresponding mid-band *VM* (*AC*) slope-sensitivity was inferred from the measured *AC/DC* ratio [17] to be $976 \times 10.44\ kV_{rms}.m_{rms}^{-1}$, or $10.18\ MV_{rms}.m_{rms}^{-1}$ (at 1.48 kHz).

At 500 Hz, on the other hand, the corresponding value was found to be $(9.43 \pm 1.20)\ MV_{rms}.m_{rms}^{-1}$, when taken over the four detectors/amplifiers, since the *AC/DC* gain ratio was 904 at this frequency. With an exceptionally low *VM AC* output noise PSD at 500 Hz of $(-64.0 \pm 0.5)\ dBV_{rms}/\sqrt{Hz}$, when taken over all four—partially shaded—detectors, and with the high *AC* slope sensitivity of the detection system, the limiting

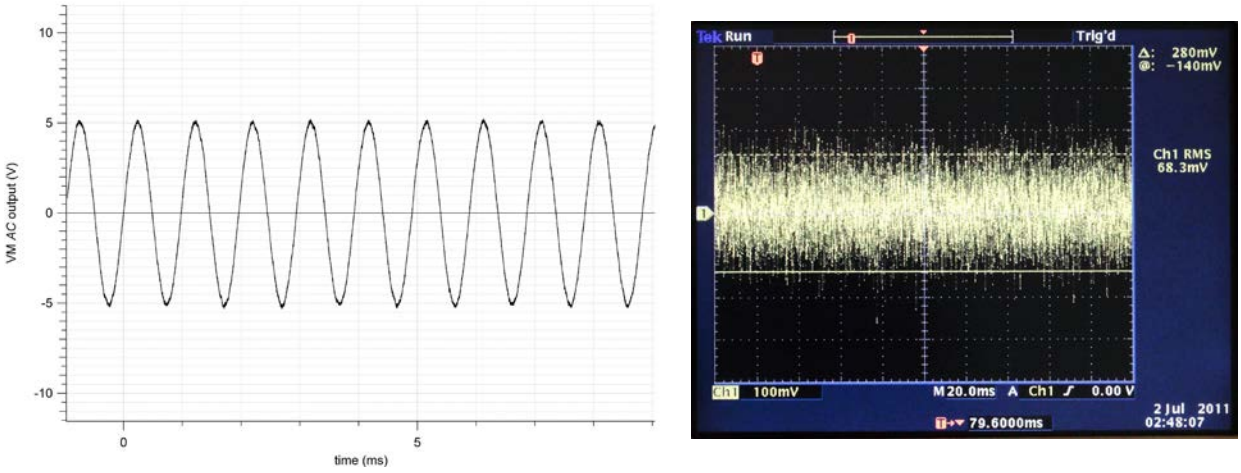

Figure 6. Left: Resonant acoustic excitation of the fundamental Violin-Mode of a 95 mm long silica fibre sample, 400 µm in diameter, using a distant loudspeaker. The resonant frequency was found to be 1.0191 kHz. A single capture of the resulting Violin-Mode waveform is shown, at approximately 10 volts, peak-peak. Therefore, the amplitude of the test fibre's transverse Violin-Mode motion was approximately 1 µm, peak-peak. Right: Photo of the Tektronix TDS-3052B oscilloscope screen, showing the amplifier's typical broadband output noise level to be ~ 68 mV (rms) at the amplifier's VM *AC* output—in agreement with theory for this wide frequency band. The horizontal bars have been set approximately at the ±2σ levels. Please refer to the text.

displacement sensitivity of the full shadow sensor/amplifier system was found to be (69 ± 13) picometres (rms) /√Hz at 500 Hz, over a measuring span of ±0.1 mm—thus exceeding its target sensitivity of $10^{-10}\ m_{rms}$ /√Hz, at this frequency, over this measuring range [7,8,9].

4. Conclusions

Both the single-input and the final differential form of the Violin-Mode amplifier turned out to be extremely low noise, with a noise level measured for the latter that was little different from the fundamental limit expected from (uncorrelated) shot noise in the two photodiode detectors. Indeed, the 'white noise' region of the differential amplifier's Power Spectral Density followed its theoretical pass-band very closely over the frequency range investigated, as seen in Figure 5, only deviating above this form for frequencies below ~ 50 Hz, where 1/f noise dominated. Both versions of the amplifier exhibited close-to the theoretically expected signal gain, with the *AC/DC* gain ratio mid-band (1.48 kHz) being very close to the expected value of approximately 1000, or +60 dB. Moreover, the signal gain at the 'pendulum-mode' frequency of ~ 0.6 Hz was, by a very useful factor of > 70,000 (97 dB), smaller than that found mid-band—allowing Violin-Mode signals in the

range 500 Hz–5 kHz to be detected, even in the presence of very much larger pendulum motion of the test mass and its supporting fibres. The differential amplifier's *AC* pass-band extended from 226 Hz to 8.93 kHz (–3 dB), and its very low noise level allowed it, in principle, to recover a 500 Hz sinusoidal Violin-Mode vibration of amplitude (69 ± 13) picometres (rms), in one second; and yet, this same amplifier output could handle, without clipping or distortion, a similar signal of amplitude 2.4 μm (or, ~23volts), peak-peak. The subsidiary '*DC*' outputs had a designed (*DC*) sensitivity to quasi-static shadow displacement that was lower than the mid-band *AC* sensitivity by a factor of approximately1000. These outputs therefore exhibited a much larger detection range for shadow displacement, with a bandwidth extending from true *DC*–160 Hz (–3 dB points), allowing pendulum-mode signals at 0.64 Hz, and of amplitude exceeding 200 μm peak-peak, to be captured, without attenuation. In summary, the differential Violin-Mode amplifier described above clearly met, or exceeded, all of its performance targets.

At the time of writing the Violin-Mode amplifier and sensor system described here has not been adopted for aLIGO, and, in fact, the issue of vacuum compatibility remains unresolved, because the *Hamamatsu* photodiodes used for the detector elements had been encapsulated, using an epoxy [15]. However, were it to become necessary, the issue of the epoxy for the photodiodes from this, or another, manufacturer probably could be resolved, and the LEDs and other components used are likely to prove compliant with the stringent requirements of aLIGO, or have vacuum-compliant alternatives.

5. Acknowledgements

We thank the IGR, University of Glasgow, Scotland, UK, for the silica fibre test samples used in this work, and acknowledge that without the research of Alan Cumming, Giles Hammond and Liam Cunningham of that institution on development and construction of the prototype aLIGO test-suspension used in obtaining the Violin-Mode results reported here, the work reported in this paper would not have been possible. We also thank Angus Bell of the IGR, Norna Robertson and Calum Torrie of Caltech and the IGR, Dennis Coyne of Caltech, Peter Fritschel, David Shoemaker, Rich Mittleman, and Brett Shapiro of MIT, Alberto Vecchio of the University of Birmingham, and Justin Greenhalgh of the CCLRC (RAL), for their oversight of, and assistance with, this work. We are grateful to John Broadfoot, Ged Drinkwater, and Mark Hutcheon of the Physics Department's Electronics Workshop, and to the staff of the Science Faculty's Mechanical Workshop, at the University of Strathclyde, for their careful construction of most of the component parts used in this work. Finally, we are grateful for the support of grant STFC PP/F00110X/1, which sustained this work.

References

[1] Harry G M (for the LIGO Scientific Collaboration) 2010 Advanced LIGO: the next generation of gravitational wave detectors. *Class. Quantum Grav.* **27** 084006 (12pp).

[2] Abbott B P *et al* 2009 LIGO: The Laser Interferometer Gravitational-Wave Observatory *Rep. Prog. Phys.* **72** 1–25.

[3] Raab F J *et al* 2004 Overview of LIGO Instrumentation *Proceedings of SPIE* **5500** 11–24 (29 Sept.).

[4] Aston S M *et al* 2012 Update on quadruple suspension design for Advanced LIGO *Class. Quantum Grav.* **29** 235004 (25pp).

[5] Heptonstall A *et al* 2011 Invited Article: CO_2 laser production of fused silica fibres for use in interferometric gravitational wave detector mirror suspensions *Rev. Sci. Instrum.* **82**, 011301 1–9.

[6] Cumming A V *et al* 2012 Design and development of the advanced LIGO monolithic fused silica suspension *Class. Quantum Grav.* **29** 035003 (18pp).

[7] Lockerbie N A, Tokmakov K V, and Strain K A 2014 A source of illumination for low-noise 'Violin Mode' shadow sensors, intended for use in interferometric gravitational wave detectors. *Document No. T1100047-v3 available at https://dcc.ligo.org/. (*TBA *MST).*

[8] Lockerbie N A and Tokmakov K V 2014 A 'Violin-Mode' shadow sensor for interferometric gravitational wave detectors. *Document No. T1100046-v3 available at https://dcc.ligo.org/. (*TBA *MST).*

[9] Lockerbie N A *et al* 2011 First results from the 'Violin-Mode' tests on an advanced LIGO suspension, at MIT. *Class. Quantum Grav.* **28** 245001 (12pp).

[10] Carbone, L., et al. 2012 Sensors and actuators for the Advanced LIGO mirror suspensions. *Classical and Quantum Gravity* 29 11 115005 (14pp).

[11] Dmitriev A *et al* 2010 Controlled damping of high-Q violin modes in fused silica suspension fibres. *Class. Quantum Grav.* **27** 025009 (8pp).

[12] Brisebois G 2008 *Linear Technology Design Note DN399*: Low Noise Amplifiers for Small and Large Area Photodiodes, available at http://cds.linear.com/docs/Design%20Note/dn399f.pdf

[13] *Burr-Brown IC Applications Handbook* 1994 OP201 Photodiode-Amplifier Rejects Ambient Light (AB-061), p. 379.

[14] Johnson M 2003 Photodetection and Measurement McGraw-Hill ISBN 0-07-140944-0, p. 146.

[15] *Hamamatsu* S2551 photodiodes: http://www.hamamatsu.com/.

[16] Lockerbie N A, Tokmakov K V A modulated Near InfraRed gain calibration system for a 'Violin-Mode' transimpedance amplifier, intended for advanced LIGO suspensions (TBA).

[17] [Lockerbie N A, Tokmakov K V 2014 A calibration system for a 'Violin-Mode' shadow-sensor in advanced LIGO suspensions (TBA).

[18] Finesse Voltage Regulator Noise! (Wenzel Associates Inc.). This document can be found at http://www.wenzel.com/documents/finesse.html.